A High-Resolution Map of Synteny Disruptions in Gibbon and Human Genomes

Lucia Carbone[1☯*], Gery M. Vessere[1☯], Boudewijn F.H. ten Hallers[1], Baoli Zhu[1], Kazutoyo Osoegawa[1], Alan Mootnick[2], Andrea Kofler[3], Johannes Wienberg[4], Jane Rogers[5], Sean Humphray[5], Carol Scott[5], R. Alan Harris[6], Aleksandar Milosavljevic[6], Pieter J. de Jong[1]

1 BACPAC Resources, Children's Hospital of Oakland Research Institute, Oakland, California, United States of America, **2** Gibbon Conservation Center, Santa Clarita, California, United States of America, **3** Chrombios GmbH, Raubling, Germany, **4** Anthropology and Human Genetics, Department of Biology II, Munich University, Munich, Germany, **5** Wellcome Trust Sanger Institute, Wellcome Trust Genome Campus, Cambridge, United Kingdom, **6** Department of Molecular and Human Genetics, Baylor College of Medicine, Houston, Texas, United States of America

Gibbons are part of the same superfamily (Hominoidea) as humans and great apes, but their karyotype has diverged faster from the common hominoid ancestor. At least 24 major chromosome rearrangements are required to convert the presumed ancestral karyotype of gibbons into that of the hominoid ancestor. Up to 28 additional rearrangements distinguish the various living species from the common gibbon ancestor. Using the northern white-cheeked gibbon (2n = 52) *(Nomascus leucogenys leucogenys)* as a model, we created a high-resolution map of the homologous regions between the gibbon and human. The positions of 100 synteny breakpoints relative to the assembled human genome were determined at a resolution of about 200 kb. Interestingly, 46% of the gibbon–human synteny breakpoints occur in regions that correspond to segmental duplications in the human lineage, indicating a common source of plasticity leading to a different outcome in the two species. Additionally, the full sequences of 11 gibbon BACs spanning evolutionary breakpoints reveal either segmental duplications or interspersed repeats at the exact breakpoint locations. No specific sequence element appears to be common among independent rearrangements. We speculate that the extraordinarily high level of rearrangements seen in gibbons may be due to factors that increase the incidence of chromosome breakage or fixation of the derivative chromosomes in a homozygous state.

Citation: Carbone L, Vessere GM, ten Hallers BFH, Zhu B, Osoegawa K, et al. (2006) A high-resolution map of synteny disruptions in gibbon and human genomes. PLoS Genet 2(12): e223. doi:10.1371/journal.pgen.0020223

Introduction

During recent years, great progress has been made in understanding the evolutionary processes governing mammalian chromosomal organization. It is now commonly accepted that the mammalian karyotype has undergone a limited number of major rearrangements over the course of more than 100 million years [1]. A few species represent an exception to the rule by demonstrating a very high incidence of karyotypic changes. Mouse, rat, and dog are often cited as examples of exceptionally rearranged chromosomes compared to the putative ancestral mammalian karyotype [2–5] The small apes or gibbons (Hylobatidae) exhibit heavily reshuffled chromosomes relative to most other members of the primate order and, most significantly, relative to other members of the superfamily Hominoidea: the great apes and humans. Humans and great apes have a karyotype more similar to the ancestral mammalian karyotype, suggesting that the chromosomal instability evolved in the ancestor of the small apes. The high rate of karyotype rearrangement persisted from the common gibbon ancestor to the current species as indicated by the four karyomorphs that define the four gibbon genera: *Symphalangus* (siamang) 2n = 50, *Nomascus* (crested gibbon) 2n = 52, *Hylobates* (Hylobates group) 2n = 44, and *Hoolock* (hoolock gibbon) 2n = 38 [6–8]. The evolutionary mechanisms that generated this karyotype diversity may have terminated or may still be in action today.

Recent studies describing the dynamics of mammalian genome evolution indicate a "reuse" of genomic regions for independent evolutionary breakpoints in different lineages as well as the presence of hotspots and fragile sites more prone to rearrangements. These fragile loci frequently coincide with regions enriched for segmental duplications (SDs) in primates and involved in human genomic disorders [9–17]. Moreover, it is well known that transposable elements are responsible for chromosomal instability in *Drosophila* [18,19] and endogenous retroviruses are involved in genome shuffling in mammals [15,20,21].

Gibbon karyotypic changes have previously been investigated by cytogenetic banding analysis [6,22–24] and more recently by comparative chromosome painting [7,8,25–29] and reciprocal chromosome painting techniques [30,31]. The maps resulting from these experiments are limited by the

Editor: Barbara J. Trask, Fred Hutchinson Cancer Research Center, United States of America

Received August 28, 2006; **Accepted** November 13, 2006; **Published** December 29, 2006

A previous version of this article appeared as an Early Online Release on November 13, 2006 (doi:10.1371/journal.pgen.0020223.eor).

Copyright: © 2006 Carbone et al. This is an open-access article distributed under the terms of the Creative Commons Attribution License, which permits unrestricted use, distribution, and reproduction in any medium, provided the original author and source are credited.

Abbreviations: BAC, bacterial artificial chromosome; BES, BAC end sequence; BOSR, break of synteny region; DOP PCR, degenerate oligonucleotide-primed PCR; FISH, fluorescence in situ hybridization; HLA, *H. lar*; HSA, *Homo sapiens*; indel, insertion/deletion; NLE, *Nomascus leucogenys leucogenys*; SD, segmental duplication

* To whom correspondence should be addressed. E-mail: lcarbone@chori.org

☯ These authors contributed equally to this work.

Synopsis

It is commonly accepted that mammalian chromosomes have undergone a limited number of rearrangements during the course of more than 100 million years of evolution. Surprisingly, some species have experienced a large increase in the incidence of rearrangements, including translocations (exchange between two non-homologous chromosomes), inversions (change of orientation of one chromosomal segment), fissions, and fusions. Within the primate order, gibbons exhibit the most strikingly unstable chromosome pattern. Gibbon chromosomal structure greatly differs from that of their most recent common ancestor with humans from which they diverged over 15 million years ago. The authors are interested in the mechanisms causing this extraordinary instability. In this study, they employed modern techniques to compare the human and white-cheeked gibbon chromosomes and to localize all the regions of disrupted homology between the two species. Their findings indicate that the molecular mechanism of gibbon chromosomal reshuffling is based on the same principles as in other mammalian species. To explain the 10-fold higher incidence of gibbon chromosomal rearrangements, it will be necessary to pursue future studies into other biological factors such as inbreeding and population dynamics.

resolution of fluorescence microscopy (about 3–5 Mb). As a result, it is difficult to correlate gibbon rearrangements detected by these methods with smaller scale genomic sequence features. A more detailed analysis of breakpoint regions may determine if the rearrangements are caused by gibbon-specific genomic sequence features. Alternatively, the breakpoints may coincide with sequence features found at rearrangement sites in other mammals, including human. To decide between these two alternatives, it is necessary to first map the numerous gibbon chromosome breakpoints at high resolution based on DNA sequence alignments and then to sequence the new junctions.

Here, we compared the karyotypes of *Nomascus leucogenys leucogenys* (NLE) (northern white-cheeked gibbon) and human using a combination of high-resolution genomic technologies: array comparative genome hybridization painting [32,33], bacterial artificial chromosome (BAC) end-sequence profiling [33], and confirmation by fluorescence in situ hybridization (FISH). Our approach made optimal use of BAC libraries from the human and gibbon genomes to create a map of 100 gibbon breakpoints relative to the human genome at a resolution of approximately 200 kb, the size of a typical BAC clone. We isolated 67 gibbon BAC clones spanning breakpoints with the intent of looking at the species-specific sequences in these regions. The full sequences of a subset of these clones provide insight into the architecture of rearranged chromosomal regions at the molecular level.

Results/Discussion

Overview of the Genomic Tools Used in the Experiments

The three main resources used in this study were 1) high-resolution microarray slides containing about 32,000 BAC clones spanning the entire human genome ("32K set"), 2) a genomic BAC library for the northern white-cheeked gibbon (CHORI-271) described in more detail at http://bacpac.chori.org/library.php?id=228, and 3) the latest genome assemblies of rhesus macaque (UCSC build rheMac2) and chimpanzee (UCSC build panTro1) used as outgroups to resolve rearrangements to the great ape or small ape lineage.

To better understand karyotype instability, gibbon-specific sequences at the break of synteny regions (BOSRs) need to be analyzed. To determine if it is possible to attribute breakpoints to specific sequence elements or to the genomic architecture of these regions, we sequenced a preliminary set of 11 gibbon BAC clones spanning BOSRs.

Breakpoint Identification by Array Painting of Flow-Sorted Gibbon Chromosomes on Human Arrays

We employed array painting (see [32] and Materials and Methods for more details) to map the end-points of gibbon–human synteny regions relative to the human genome. In this technique the chromosomes carrying balanced reciprocal translocations are isolated by flow sorting, and the DNAs are labeled with two contrasting dyes (Cy3 and Cy5) and hybridized to an array of 32,000 human BAC DNAs spotted on a glass slide. A single hybridization thus permits the accurate mapping of breakpoints at a resolution determined by the genomic intervals between BACs on the array. A breakpoint detected by this method is referred to as a BOSR.

Optimal experimental conditions were found by hybridizing three gibbon chromosomes separately (NLE13, NLE20, and NLE10) in a preliminary array-painting experiment. Array-painting experiments were then economized by pooling the sorted gibbon chromosomes so that the gibbon chromosomes in each pool detected distinct human chromosomes. This "smart pooling" was possible because the gibbon–human synteny regions have previously been identified through chromosome painting [7,28,29,31]. Pooling allowed us to conduct array painting on four pools of gibbon chromosomes, which was equivalent to conducting 26 separate hybridizations for each gibbon chromosome ($2n = 52$). The pooling strategy is shown in Table S1.

Single test and reference hybridization results revealed that the signal-to-noise ratio was too low for accurate detection of BOSR coordinates. After determining that the hybridization noise was systematic, we developed a noise-reduction method (Protocol S1) to obtain better definition of the breakpoints. Figure 1A and 1B shows the individual data plots for human Chromosome 2 obtained with pools containing flow-sorted chromosomes NLE14 and NLE19, respectively. These two gibbon chromosomes resulted from a reciprocal translocation and many inversions involving ancestral sequences homologous to human Chromosomes 2 and 17 [7]. After applying our noise-reduction method, we obtained a well-defined shift in the plateau values at a single location coinciding with the approximate site of the BOSR (Figure 1C). Results for all reciprocal BOSRs pairs are presented in Figure S1.

Altogether, 64 BOSRs have been mapped to the human genome (Hg17, UCSC May 2004) (Table 1 and Figure 2). Among these 64 regions, four correspond to human centromeres and one overlaps with the site where two ancestral ape chromosomes fused telomere-to-telomere to form human Chromosome 2 (2q13-2q14). Six noncentromeric BOSRs (BOSR-33, -41, -44, -45, -52, and -61) could not be mapped with a precision higher than 850 kb. In the case of BOSR-33 and BOSR-45, mapping resolution was affected by their pericentromeric locations where abundant human genomic duplications caused noisy plots. In the

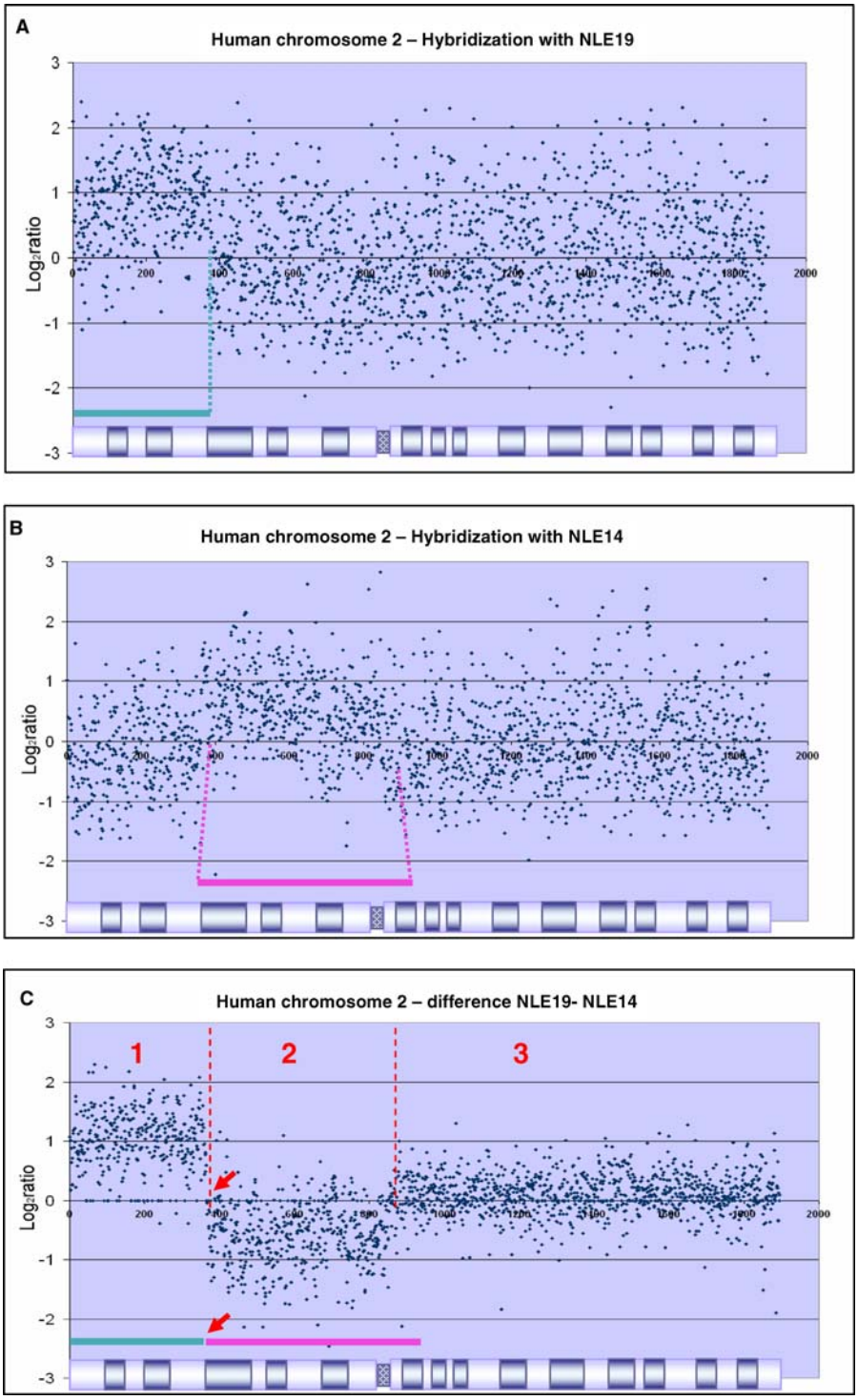

Figure 1. Identification of Break of Synteny Regions Using the Log_2 Ratio Difference Method

(A and B) The plotted value of Log_2 ratio/chromosome length for human Chromosome 2 after hybridization with sorted gibbon chromosomes NLE14 and NLE19, respectively.

(C) Results of the application of the difference method to the datasets in (A) and (B). After canceling out the systematic variation, it is possible to discern three different regions from left to right, one amplified (1), one deleted (2), and one at the baseline (3).

doi:10.1371/journal.pgen.0020223.g001

particular case of BOSR-44, we confirmed that the high noise resulted from a neighboring keratin-associated protein gene cluster located on human chromosome 11q13.5 (data not shown).

FISH Confirmation and Cross-Species Analysis of BOSRs

In order to confirm the accuracy of array-painting results, ten BOSRs were validated by FISH experiments where BAC clones from the "32K set" were hybridized to NLE metaphase

Table 1. Array-Painting Results

BOSR ID	Gibbon Chromosomes	Human Chromosome	Position (UCSC May 2004)	Interval (bp)	BOSR ID	Gibbon Chromosomes	Human Chromosome	Position (UCSC May 2004)	Interval (bp)
1	24–12a	Chr1	29973196–30505910	532,714	33	8d-16	Chr8	47902612–49272605	1369,993
2	12a-5a	Chr1	51896962–52415128	518,166	34	1(b)a-8f	Chr9	22149708–22522776	373,068
3	5a-12b	Chr1	66926758–67624390	697,632	35	8f-1(b)b	Chr9	27020088–27353114	333,026
4	12b-9b	Chr1	177536856–178131163	594,307	36	1(b)b-8g	Chr9	28846361–29324149	477,788
5	9b-5b	Chr1	200720381–201190768	470,387	37	8g-1(b)c	Chr9	45719577–68429077	22709,5
6	19e-14e	Chr2	47437262–47762798	325,536	38	1b(c)-8h	Chr9	111110463–111480794	370,331
7	14e-20a	Chr2	113552493–113956226	403,733	39	9d-18b	Chr10	23544826–24115999	571,173
8	20a-17e	Chr2	150118398–150461545	343,147	40	18b-3a	Chr10	51442401–51788808	346,407
9	17e-22(b)d	Chr2	168973521–169384482	410,961	41	3a-18c	Chr10	56628164–58307523	1679,359
10	21a-8b	Chr3	14928673–15399978	471,305	42	18c-3b	Chr10	88734014–89428545	694,531
11	8b-4c	Chr3	19874977–20167322	292,345	43	15a-4b	Chr11	51314556–54999407	3684,851
12	4c-21b	Chr3	58517748–58812691	294,943	44	4b-15b	Chr11	69306850–71048199	1741349
13	21b-8c	Chr3	131250104–131525418	275,314	45	23–11d	Chr12	36144431–37011428	866,997
14	8c-11f	Chr3	147534898–148015319	480,421	46	11d-8a	Chr12	45475193–45779410	304,217
15	20b-9c	Chr4	49329887–49472520	142,633	47	8a-11e	Chr12	52494400–52720255	225,855
16	9c-18d	Chr4	110520763–110838079	317,316	48	11e-10c	Chr12	63328829–63614208	285,379
17	18d-7b	Chr4	116816109–117629834	813,725	49	5c-9a	Chr13	25994386–26512210	517,824
18	7c-18e	Chr5	54108773–54459262	350,489	50	9a-5d	Chr13	39131766–39352944	221,178
19	18e-2a	Chr5	75543667–75840386	296,719	51	22(b)a-1(b)e	Chr14	30571348–31256565	685,217
20	8e-1(b)d	Chr6	26745083–27138455	393,372	52	1(b)e-22(b)b	Chr14	72215467–73414172	1198,705
21	1(b)d-17f	Chr6	36216526–36547325	330,799	53	18a-2b	Chr16	19290200–19589554	299,354
22	17f-22(b)c	Chr6	46136459–46542950	406,491	54	19a-14a	Chr17	16592363–17035446	443,083
23	22(b)c-3c	Chr6	57356628–57614844	258,216	55	14a-19b	Chr17	22320285–22831140	510,855
24	3c-18f	Chr6	78789403–79038560	249,157	56	19b-14b	Chr17	27322899–27707130	384,231
25	18f-3d	Chr6	85854470–86291702	437,232	57	14b-19c	Chr17	30342581–30645726	303,145
26	17e-11b	Chr7	6445059–6900407	455,348	58	19c-14c	Chr17	45862411–46255459	393,048
27	11b-17b	Chr7	23350766–23824362	473,596	59	14c-19d	Chr17	57343941–57719599	375,658
28	17b-13c	Chr7	76242931–76674207	431,276	60	19d-14d	Chr17	61469371–61864837	395,466
29	13c-11c	Chr7	79628730–79945696	316,966	61	10a-17d	Chr19	42743440–43727640	984,2
30	11c-17c	Chr7	96960514–97292680	332,166	62	17d-10b	Chr19	51436748–51826573	389,825
31	17c-13d	Chr7	101574440–101913114	338,674	63	13a-11a	Chr20	5320992–5573692	252,7
32	4d-8d	Chr8	19702748–20125589	422,841	64	11a-13b	Chr20	16373549–16720741	347,192

The table lists BOSRs between human and gibbon identified by array painting. The location on the human genome corresponds to the Hg17 assembly. The BOSR IDs correspond to Figure 2.

doi:10.1371/journal.pgen.0020223.t001

preparations. In most of the cases, a single BAC hybridized to two disparate locations as expected. Only BOSR-32 and BOSR-11 demonstrated a single hybridization signal, suggesting that the breakpoint was located between two BACs or in a small region of overlap between them. A few examples of FISH experiments are shown in Figure 3A.

Additionally, six of these BOSRs, thought to be common to all gibbons [7,29], were mapped to the gibbon species *Hylobates lar* (HLA) (2n = 44) using the same human FISH probes (Figure 3A). In five cases (BOSRs –8, –16, –19, –35 and –53), the human BACs produced similar split signals on HLA and NLE metaphase preparations, indicating that the breakpoint is shared by the two species, strengthening the original hypothesis that the breaks occurred in the karyotype of a common ancestor [7,29]. However, in one case (BOSR-6), we did not observe a split FISH signal on the HLA metaphase preparations (data not shown). This result suggests that this translocation occurred in the NLE lineage after the split from the common ancestor of NLE and HLA.

Breakpoint Identification by Gibbon BAC End Sequence Mappings onto Human

Both ends of 5,376 clones from the gibbon genomic BAC library CHORI-271 were sequenced and mapped onto the human genome using the BLAT program [34] (Protocol S1). Gibbon BACs spanning putative breakpoints were identified using the paired BAC end-sequence mappings to the human genome by applying a "pairing criteria" implemented as a script (Protocol S1). Mapping results are summarized in Table 2.

For the purpose of visualizing the gibbon clones mapped onto the human genome, we created a software tool that graphically depicts the chromosomal position of gibbon BAC mappings on the human genome. This software allows for full chromosome views as well as views showing a user-configurable window size (Protocol S1 and Figure S2A and S2B). This tool allowed us to easily overlay the BAC end sequence (BES) mappings onto mappings obtained from array painting and manually identify additional clones.

Figure 2. Comparative Map of Human and Gibbon Chromosomes

Ideogram of human chromosomes with orthologous gibbon chromosomes identified by array painting represented by colored bars to the left of each chromosome. Each segment is named after the gibbon chromosome followed by a small letter that refers to its mapping order in the gibbon chromosome. The BOSRs have been defined for convenience by numbers (Table 1). Gibbon clones spanning breakpoints identified by BES mapping are also located on the map. Clones with map positions that disagree with the array-painting map are italicized.

doi:10.1371/journal.pgen.0020223.g002

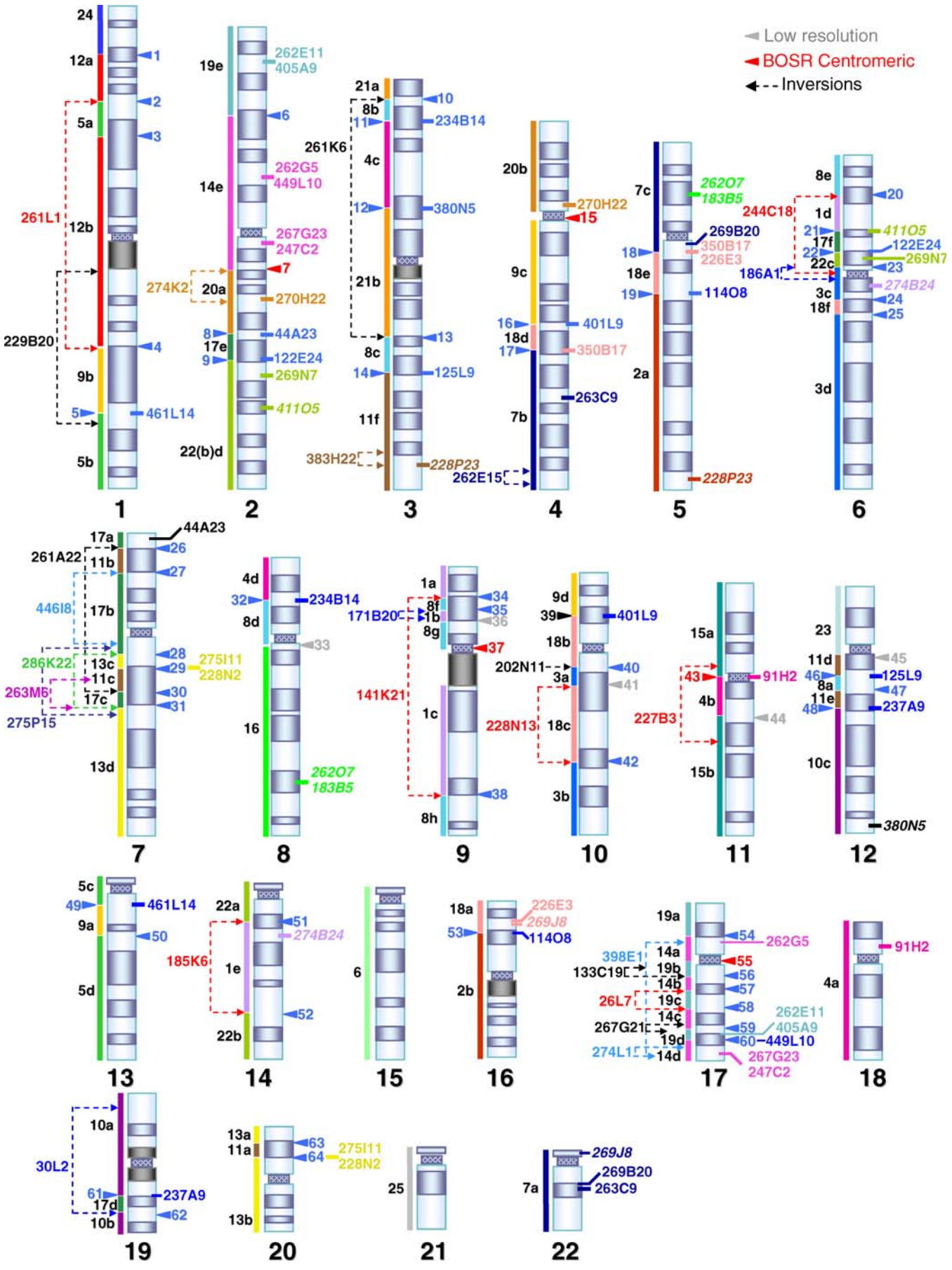
Low resolution
BOSR Centromeric
Inversions
1
2
3
4
5
6
7
8
9
10
11
12
13
14
15
16
17
18
19
20
21
22

Interchromosomal Rearrangements

Gibbon clones identified as putatively spanning interchromosomal rearrangements were mapped by FISH on gibbon metaphase preparations. Clones giving signals on more than two gibbon chromosomes were considered possible clone artifacts (chimeric clones) or duplicated regions in the gibbon and were removed from further analysis. We also screened the gibbon BAC CHORI-271 library (Materials and Methods) in order to identify at least two additional clones spanning identified breakpoints. Table 3 reports clones that were validated by combining the array-painting, FISH, and library-screening approaches. Twenty-five clones were confirmed by additional overlapping clones with BES mappings to the same pair of human chromosomes. In seven instances, we identified clones spanning reciprocal breakpoints by library screening and subsequent BES. These clones map on the same region of the human genome; however, they are localized on two derivative gibbon chromosomes in the case of translocations, or different regions of the same chromosome in the case of inversions. We verified that these clones carry reciprocal breakpoints by FISH hybridization on gibbon metaphases. Examples of FISH experiments are shown in Figure 3B.

Intrachromosomal Rearrangements

Based on our pairing criteria, most of the clones identified as spanning intrachromosomal rearrangements resulted from insertion/deletions (indels) in either the gibbon or the human genomes (74 out of 97). Indels cause discrepancies between paired BES mapping distances on the human genome compared to the average gibbon BAC insert size. We formally defined this as BES mappings at a distance less than or greater than three standard deviations from the 172-kb-clone insert size. We verified the insert size of the 74 clones spanning putative indels using NotI digestion and pulsed-field electrophoresis. Based on the pulsed-field electrophoresis, the 60 gibbon BACs with BES mapping distances of 40–60 kb relative to the human genome were found to not be indels, as they had actual insert sizes in the 40–60 kb range. We presumed that the remaining 14 clones with BES distances exceeding 300 kb represent actual insertions in the human genome or deletions in the gibbon genome. Results are summarized in Table 4.

Clones putatively spanning inversion breakpoints were validated by comparisons with BOSRs previously defined by array painting (Table 3). Large-scale inversions were further confirmed by hybridizing the gibbon clones onto human metaphase preparations (Figure 3C). Additional clones spanning the same breakpoint were obtained by screening the CHORI-271 library as described for interchromosomal breakpoints. Through this validation process, 15 out of 23 clones were confirmed and the remaining eight clones were removed from consideration.

Combination of Array Painting and End-Sequencing Mapping

The goals of our study were 1) to obtain a map of the BOSRs between human and gibbon at high resolution and 2) to identify species-specific clones spanning chromosomal rearrangements for use in further molecular analysis. In pursuit of our second goal, we selected for further analysis 38 gibbon BAC clones corresponding to BOSRs identified by array painting human BACs. We constructed probes across these BOSRs at 75-kb intervals based on the human genome sequence and used these probes to screen the gibbon library. Using this approach, we identified an additional 26 gibbon clones containing breakpoint loci (15 inversions and 11 translocations) (Table 5).

Identification of Breakpoints Specific to the Gibbon Lineage

To ensure that we identified rearrangements that occurred in the gibbon lineage, we mapped the BES of gibbon clones identified as spanning rearrangement breakpoints onto the latest genome assemblies of rhesus macaque (UCSC Build rheMac2) and chimpanzee (UCSC Build panTro1) using BLAT. We removed ambiguous mappings and classified the remaining mappings using the same pairing criteria applied to the human genome mappings. We classified putative rearrangements as 1) gibbon specific if gibbon was rearranged relative to human, chimpanzee, and macaque; 2) great ape specific if gibbon was not rearranged relative to macaque, but was rearranged relative to human and chimpanzee; and 3) human specific if gibbon was not rearranged relative to macaque and chimpanzee but was rearranged relative to human (Table S2). Based on this classification, we identified three human-specific rearrangements and four great ape–specific rearrangements.

One of the events classified as great ape–specific is the inversion of human Chromosome 3, with breakpoints at 3p25 and 3q21, which are regions already known as rearrangement hotspots in primates [35]. BOSR-10 and BOSR-13 from the array-painting map span these inversion breakpoints, and clone CH271-261K6 spans one of the breakpoints. Additionally, we identified a clone spanning the breakpoint of an inversion that occurred in the ancestor of the great apes in the chromosome homologous to human Chromosome 7. Müller et al. [36] previously described this inversion, which occurred in the lineage leading to human and African great apes. Human, chimpanzee, and gorilla therefore share the same derivative form, while orangutan, small apes, and macaque share the ancestral one.

In total, we identified 110 breakpoints between human and gibbon chromosomes due to intra- and interchromosomal rearrangements. Of those, 100 occurred during the evolution of the gibbon.

Figure 3. Breakpoint Validation by FISH

(A) FISH experiments to validate breakpoints identified by array painting. Images 1 and 2 show hybridization on NLE metaphase preparations with human BACs spanning breakpoints identified by array painting. The yellow color in image 1 is due to the overlap of red and green spots as both BACs map on the same chromosome. Image 3 shows a similar experiment done on HLA metaphase preparations. The reciprocal position of the BACs used in each experiment is shown in the boxes below the images.

(B) FISH validation experiments on six gibbon BAC clones spanning three reciprocal breakpoints for the same rearrangement. In the diagrams, the rearrangements are illustrated starting from the ancestral chromosome form. Abbreviation: AC, ancestral chromosome.

(C) Gibbon BACs spanning inversion breakpoints were tested by FISH on human and gibbon metaphases. A BAC spanning an inversion in gibbon is expected to give a split signal on the human chromosome and a single signal on the corresponding gibbon chromosome.

doi:10.1371/journal.pgen.0020223.g003

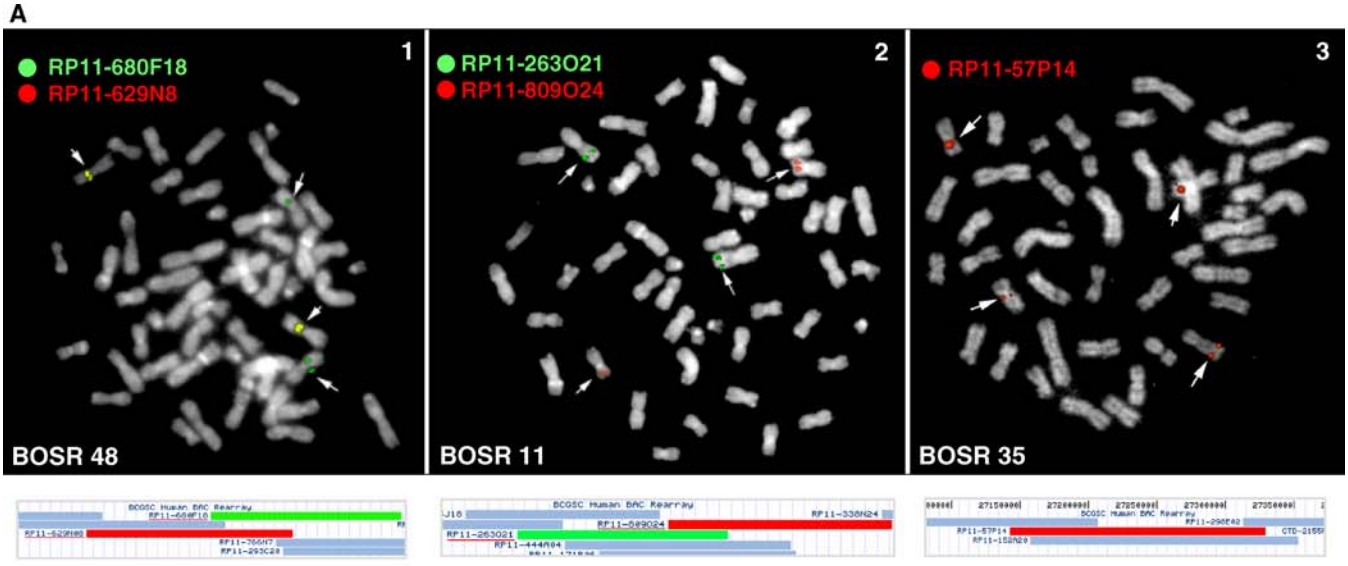
A
RP11-680F18
RP11-629N8
1
BOSR 48
RP11-263O21
RP11-809O24
2
BOSR 11
RP11-57P14
3
BOSR 35

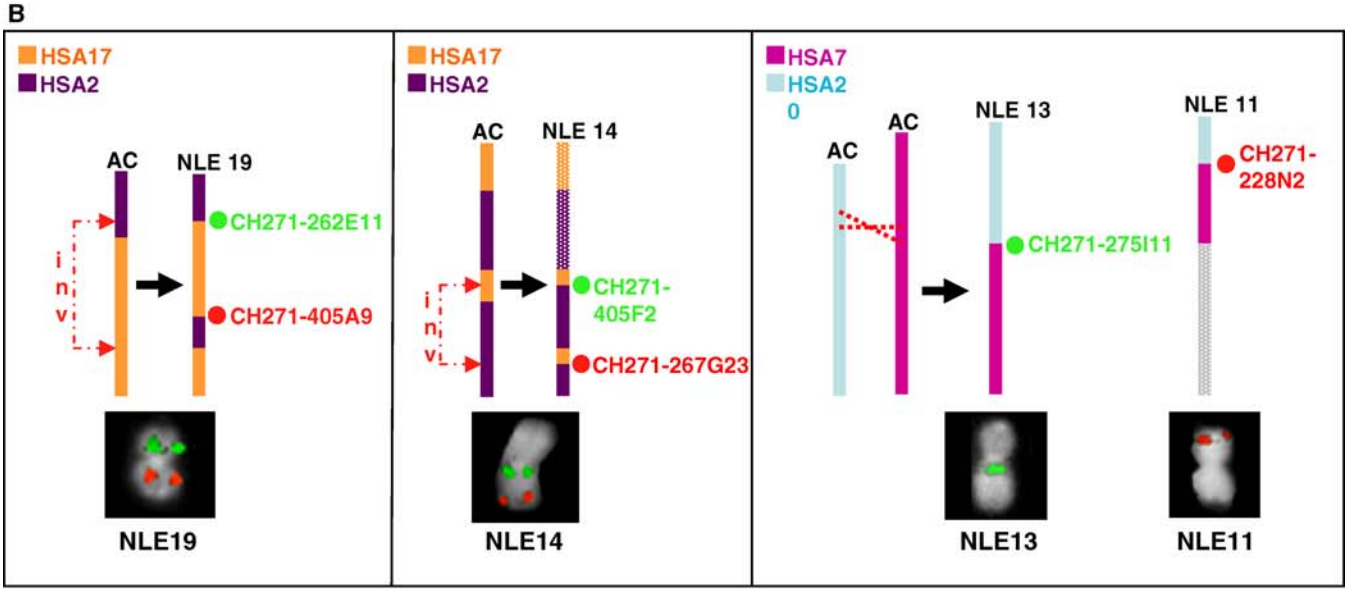
B
HSA17
HSA2
AC
NLE 19
CH271-262E11
CH271-405A9
inv
NLE19
HSA17
HSA2
AC
NLE 14
CH271-
405F2
CH271-267G23
inv
NLE14
HSA7
HSA2
0
AC
AC
NLE 13
CH271-275I11
NLE 11
CH271-
228N2
NLE13
NLE11

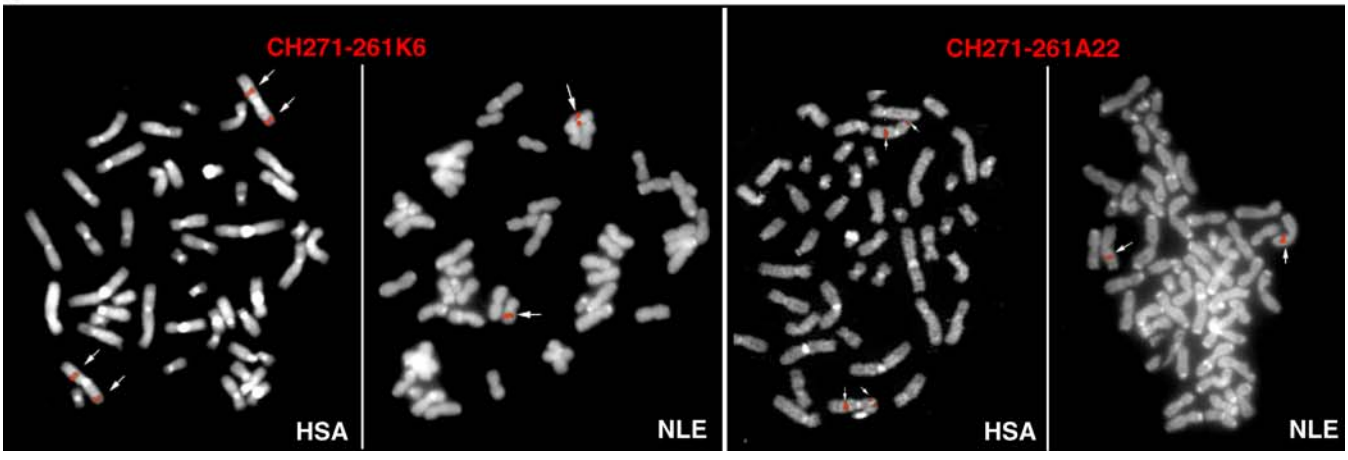
C
CH271-261K6
HSA
NLE
CH271-261A22
HSA
NLE

Analysis of Gibbon-Specific Breakpoints Spanning Regions on the Human Genome

It is widely accepted that regions of chromosomal instability and SDs colocalize more frequently than expected by random chance. SDs are blocks of DNA 1–400 kb in length, repeated in the genome with a high level of sequence identity (>90%) [37]. The association between SDs and evolutionary breakpoints in primates has been repeatedly reported [13,14,16,36,38], leading to speculation that these large blocks of homology predispose the flanking regions to rearrangement by nonallelic homologous recombination. Obviously, one would like to explore correlations between gibbon SDs and chromosomal rearrangements. Since the gibbon genome has not been sequenced, we used the human genome as the most closely related surrogate. Our assumption is that chromosomal regions enriched for SDs in gibbon may also show an enrichment of SDs in the human genome.

We first analyzed the overlap between the human regions orthologous to gibbon-specific BOSRs and the human SDs reported in the UCSC browser [39]. We found that 46 of 100 regions (46%) overlapped with at least one SD. This correlation remained strong (42%) when breakpoints located in the centromeric regions and regions identified with lower resolution were removed from the analysis. It is important to note that the BOSRs represent segments that are, on average, 220 kb. Therefore, the SD may overlap with the BOSR, but not necessarily include the actual breakpoint.

To statistically validate the significance of these data, a simulation was run in which the 100 breakpoint regions were randomly relocated 1,000 times in their original chromosome, emulating a random-breakage model (Protocol S1). The result was a count of the number of regions overlapping SDs at each step of the simulation. The association of 100 detected breakpoint regions with SDs fell more than three standard deviations away from the mean of the simulated sampling distribution (Figure 4A), indicating that this association is highly unlikely to have occurred by chance.

Measuring overlap alone does not sufficiently express the proximity of these regions to SDs; thus, the breakpoint regions were expanded in 100 kb increments and monitored for variation in the number of regions overlapping with SDs (Figure 4B). Out of the 100 regions, 80 overlapped with SDs after being expanded by 500 kb and 97 after being expanded by 1.5 Mb. We confirmed that such an overlap was unlikely to occur by chance by simulating randomly relocated regions expanded in a similar manner (data not shown). Finally, the association between our breakpoints and SDs was examined by measuring their base-pair overlap while shifting the breakpoint regions up to 5 Mb upstream and downstream of their original positions using 100 kb increments. The overlap was highest when the breakpoints were in their original positions and overlap progressively decreased with an increase in the distance shifted (Figure 4C).

Of the 46 BOSRs overlapping with human SDs, 27 are covered by at least one gibbon clone. We used these clones for interphase FISH experiments on NLE. In 22 cases, multiple signals were evident on NLE nuclei, suggesting duplicated regions. The remaining five clones showed no indication of duplications at the cytogenetic level. Additionally, 10 out of these 22 clones were duplicated in two other species of gibbon (*Symphalangus syndactylus* and HLA) belonging to different genera. These data suggest that the SDs most likely appeared within a common ancestor (Figure S3).

We cannot assume that these duplications were responsible for the chromosomal rearrangement events in NLE, as we have insufficient data to indicate the duplications predated the breakage events. However, this correlation is consistent with a well-established model in which duplications are indicative of the "plasticity" of a region [21].

Analysis of Fully Sequenced Gibbon BACs Spanning Rearrangement Breakpoints

We analyzed the finished sequence of 11 gibbon clones comprising a representative sample of the clones identified in this study. Although the rearrangement events occurred in ancestral chromosomal sequences that are in part altered in the current genome, the study of orthologous sequences can nevertheless still provide us with information about the nature of the genomic instability present in these regions. The breakpoint spanned by each clone was localized to the break of synteny between the gibbon clone and the human genome.

The first interesting discovery to emerge from the analysis of sequenced clones was the presence of "micro-rearrangements" that fell below the resolution of the BES mappings. Micro-rearrangements were observed in two clones, CH271-

Table 2. Analysis Using the Pairing Criteria of Gibbon BES Mapped on the Human Genome

Clones		Types of Clones	Number of Clones
Total clones sequenced			5,376
Clones that could not be mapped		Poor quality reads	198
		Single end mapped	1,522
Mapped clones	Multiply mapped clones	Paired clones	3,247
		Interchromosomal	287
		Intrachromosomal	122
	Uniquely mapped clones	Interchromosomal	29
		Intrachromosomal indels	74
		Intrachromosomal inversions	23

The table illustrates the results of the analysis of the gibbon BESs mapped onto the human genome. Some BACs were not informative because either one end (198) or both ends (1,522) could not be mapped. Such mapping failures resulted from low quality reads or the absence of unique sequences. Depending on the orientation and distance of the BES pairs (see text), each clone was classified as paired, interchromosomal, or intrachromosomal. We also required that each clone spanning a putative breakpoint had only a single mapping of each end. On the basis of this more stringent criterion, we classified these clones as "uniquely mapped."

doi:10.1371/journal.pgen.0020223.t002

Table 3. Gibbon BAC Clones Spanning Breakpoints Identified by Mapping End Sequences

BLAT Hits	Clone	Breakpoint	Mapping on Human Genome		Validation		
			BES 1 UCSC (Hg17)	BES 2 UCSC (Hg17)	FISH	Array Painting	Overlapping or Reciprocal Clones
Single BLAT hit							
	CH271-261L01	InvHSA1	Chr1:52090040–52090497	Chr1:177879393–177879781	HSA1p32–1?	BOSR 2–4	—
	CH271-229B20	InvHSA1	Chr1:141482391–141483204	Chr1:203067770–203066953	—	—	Overlapping CH271-263D23
	CH271-263D23	InvHSA1	Chr1:141500962–141501687	Chr1:203078984–203078484	—	—	Overlapping CH271-229B20
	CH271-261K06	InvHSA3	Chr3:131140276–131141065	Chr3:15040075–15040867	HSA3p25-3q21	BOSR 10–13	—
	CH271-262E15	invHSA4	Chr4:185452384–185451548	Chr4:187341410–187339042	—	—	1Ov
	CH271-261A22	InvHSA7	Chr7:6909033–6908294	Chr7:97013807–97014540	HSA7p22-q21	BOSR 26–30	—
	CH271-263M06	invHSA7	Chr7:92801747–92802246	Chr7:102099647–102100414	—	—	2Ov
	CH271-267G21	invHSA17	Chr17:55284621–55285294	Chr17:57642888–57643214	—	BOSR 59	2Ov
	CH271-274L01	invHSA17	Chr17:66672271–66671502	Chr17:69721057–69720629	—	—	4Ov
	CH271-230F13	HSA2–11/6	Chr2:195419232–195419924	Chr11:93109878–93112147	HLE22	—	2Ov
	CH271-269N07	HSA2–6	Chr2:180572342–180573081	Chr6:51799120–51798359	HLE22	—	—
	CH271-226E3	HSA5–16	Chr16:16097993–16097455	Chr5:54005967–54006698	HLE18	BOSR18	RecCH271-269J8 and 6Ov
	CH271-274B24	HSA6–14	Chr6:67341892–67342683	Chr14:32546513–32547325	HLE1 (tel)	discordance	2Ov
	CH271-275I11	HSA20–7	Chr20:16747495–16746766	Chr7:79689194–79689921	HLE13	BOSR 29–63	3Ov
	CH271-288N2	HSA20–7	Chr20:16545814–16546569	Chr7:79823415–79822697	HLE11	BOSR 29–63	Rec275I11, 2Ov
	CH271-228C01	HSA20–7	Chr20:16651858–16651083	Chr7:79596388–79597152	HLE13	BOSR 29–64	Overlapping CH271- 275I11
	CH271-262O07	HSA8–5	Chr8:116011453–116012115	Chr5:20660955–20661663	HLE16p	discordance	—
	CH271-183B5	HSA8–5	Chr8:115974044–115974755	Chr5:20660955–20661702	HLE16q	—	Rec262O7
	CH271-269J08	HSA16–22	Chr16:16033939–16034752	Chr22:15821435–15820704	HLE18 (cen)	discordance	1Ov
	CH271-262E11	HSA17–2	Chr17:59260052–59260792	Chr2:27718116–27718928	HLE19p	—	6Ov
	CH271-405A9	HSA17–2	Chr17:59333868–59333191	Chr2:27994865–27994148	HLE19q	—	1Ov
	CH271-262G05	HSA17–2	Chr17:20760201–20759787	Chr2:73499254–73499953	HLE14	—	1Ov
	CH271-267G23	HSA17–2	Chr17:77747544–77748535	Chr2:99432574–99431876	HLE14q	—	1Ov
	CH271-247C2	HSA17–2	Chr17:77943273–77942883	Chr2:99285457–99286181	HLE14cen	—	Rec267G23 and 4Ov
	CH271-228P23	HSA5–3	Chr5:175546944–175548051	Chr3:196976902–196977133	—	discordance	—
	CH271-263C09	HSA22–4	Chr22:32004833–32004498	Chr4:140701659–140702431	HLE7	—	4Ov
Multiple BLAT hits							
	CH271-228N13	InvHSA10	Chr10:56218669–56219382	Chr10:88936450–88935739	HSA10p11-q22	BOSR 41–42	—
	CH271-275P15	InvHSA7	Chr7:72452209–72452028	Chr7:99427263–99427604	HSA7q11.2-q22	—	3Ov
	CH271-274K2	InvHSA2	Chr2:128218474–128217676	Chr2:131949539–131950003	HSA2q14.3-q21.1	—	1Ov and Ov CH271-270H22
	CH271-270H22	HSA2–4	Chr2:131787947–131787214	Chr4:48816153–48816872	HLE20	BOSR 15	3Ov
	CH271-246M2	HSA2–17	Chr2:73408992–73409723	Chr17:20231923–20231185	HLE14	—	Overlapping CH271-262G5
	CH271-269B20	HSA5–22	Chr5:52731034–52731746	Chr22:33350231–33350648	HLE7	—	6Rec with CH271-269J8
Additional clones							
	CH271-411O5	HSA2–6	Chr2:195380759–195381309	Chr6:35729607–35729246	HLE22b	BOSR21	1Ov; Ov CH271-230F13
	CH271-350B17	HSA4–5	Chr4:117170986–117171703	Chr5:54237257–54236536	HLE18	BOSR17–18	1Ov
	CH271-91H2	HSA11–18	Chr11:54785823–54785088	Chr18:11613257–11613774	—	BOSR42	2Ov
	CH271-78K20	HSA4–16	CHr4:117475357–117475997	Chr16:68576978–68577856	—	—	1Ov
	CH271-383H22	InvHSA3	Chr3:194767754–194767106	Chr3:196994274–196993696	—	—	1Ov

List of the gibbon BACs with inversion or translocation breakpoints and their map position in the human genome. The list only includes clones that have been validated through two or more different methods: FISH, correspondence with the array-painting map, or presence of overlapping clones spanning the same breakpoint (Ov) and/or clones spanning reciprocal breakpoints (Rec). In some cases, the BES results did not agree with the array painting map (discordance).

doi:10.1371/journal.pgen.0020223.t003

372B11 and CH271-236L11, in which the complete sequence revealed regions orthologous to human chromosomes other than those predicted by BES or array painting (Figure 5). In both cases, one of the breakpoints was found to be enriched for SDs, while the other breakpoint fell within an interspersed repeat-rich region (Figure 5). This finding suggests that the gibbon genome might be more rearranged than previously observed. Our sample therefore contained 15 breaks of synteny to be analyzed rather than 11.

Five BOSRs, including the two BOSRs mentioned above, were within 5 kb of SDs. One example is the clone CH271-262E11 mapping to NLE Chromosome 19 and spanning a breakpoint between human Chromosomes 2 and 17. The BOSR in this clone was identified at the base-pair level and was found to be adjacent to the growth-hormone gene cluster. The breakpoint is 20 bp away from a duplicated segment containing the ortholog of gene *GH2*. At an approximate 2-kb distance from *GH2*, we found a block of about 15 kb duplicated in tandem. This block corresponds to a SD in the human genome located at Chr17:59292722–59308474 that is repeated in the nearby genomic region Chr17:59316565–59331044 (Hg17, UCSC May 2004). These duplications contain a second gene from the growth hormone cluster (*CHS2*). It has been shown [40] that the growth hormone family experienced an enhanced rate of duplication in primates compared to other mammals, with many duplication events occurring before the divergence of Old World monkeys and New World monkeys. Furthermore, Ye et

Table 4. Gibbon BAC Clones Spanning Indels

Indel	Clone	BES1 (UCSC, Hg17)	BES2 (UCSC, Hg17)	Size (kb)	Annotations
1	246G05	Chr10:18269232–18268552	Chr10:17811348–17812155	457	*MRC1* gene (duplicated in tandem in human)
2	230O09	Chr9:27710815–27710331	Chr9:27271497–27272252	439	
3	270C01	ChrX:64028319–64027581	ChrX:63594273–63595030	434	
4	262A11	Chr12:46440964–46440347	Chr12:46012628–46014971	428	
5	230C11	Chr1:163608469–163607729	Chr1:163182211–163182957	426	
6	270L16	Chr4:119647441–119648195	Chr4:120063804–120063049	416	SDs
7	269P20	Chr9:133866822–133867584	Chr9:134275988–134275219	409	
8	269K13	Chr1:244067762–244068481	Chr1:244423096–244422305	355	Olfactory receptor genes cluster (1q44)
9	261P07	Chr11:104216227–104216839	Chr11:104565860–104565235	349	Caspase gene cluster (11q22.3)
10	230E01	ChrX:154214505–154213745	ChrX:153900729–153901465	313	SDs
11	246A03	Chr2:83233988–83227148	Chr2:82926227–82926794	307	
12	273L4	Chr14:40115187–40115781	Chr14:40705452–40704972	590	
13	273P17	Chr4:31750176–31749402	Chr4:31418003–31418813	332	
14	263E10	Chr7:94963716–94964512	Chr7:94970070–94969290	6	

These clones were identified because their end sequence mappings suggested their size exceeded the average insert size of the library by more than three standard deviations (with the exception of clone CH271-263E10). In some cases, the indel interval corresponds to a region known to be extremely dynamic and having likely undergone duplications during recent evolution. This is the case for the olfactory receptor and caspase gene clusters (see Annotations column).
doi:10.1371/journal.pgen.0020223.t004

al. [40] recently showed that the NLE growth hormone cluster behaved differently from other primates, with rapid evolution occurring after the divergence of the gibbon ancestor from the great apes. The coexistence of duplications and an inversion breakpoint indicate this region is highly unstable and may be one of the rearrangement hotspots of primate genomes.

Six of the BOSRs coincided with interspersed repeats (SINEs, LINEs, and LTRs). In clone CH271-236L11, an alpha-satellite was identified due to the proximity of the BOSR to a

Table 5. Gibbon BAC Clones Isolated Using the Array-Painting Map Combined with Filter Screening and BES Mapping

Clone	Breakpoint	Mapping on Human Genome		Validation	
		BES 1 UCSC (Hg17)	BES 2 UCSC (Hg17)	Array Painting	Overlapping or Reciprocal Clones
CH271-461L14	HSA1–13	Chr1:200502116–200501557	Chr13:26172852–26173025	BOSR5–49	4Ov
CH271-122E24	HSA2–6	Chr2:168951090–168951524	Chr6:46093242–46093649	BOSR9–22	1Ov
CH271-40A18	HSA2–6	Chr2:169109259–169109013	Chr6:46409575–46409436	BOSR9–22	RecCH271-122E24 and 1Ov
CH271-44A23	HSA2–7	Chr2:150270219–150270174	Chr7:2508091–2507940	BOSR8	1Ov
CH271-449L10	HSA2–17	Chr2:73525815–73525741	Chr17:61790104–61789574	BOSR60	—
CH271-234B14	HSA3–8	Chr3:19775973–19776048	Chr8:20170234–20169964	BOSR11–32	1Ov
CH271-380N5	HSA3–12	Chr3:58788155–58788378	Chr12:120345686–120344950	BOSR12	—
CH271-125L9	HSA3–12	Chr3:147741227–147740540	Chr12:45808180–45808565	BOSR14–46	—
CH271-401L9	HSA4–10	Chr4:110750313–110750205	Chr10:24076771–24076626	BOSR16–39	—
CH271-114O8	HSA5–16	Chr5:75773648–75772974	Chr16:19526628–19525951	BOSR19–53	1Ov
CH271-237A9	HSA12–19	Chr12:63623342–63622791	Chr19:41730158–41730776	BOSR49–61	2Ov
CH271-186A1	InvHSA6	Chr6:57494813–57495068	Chr6:62082493–62082541	BOSR23	—
CH271-141K21	InvHSA9	Chr9:22218730–22218920	Chr9:111444480–111444616	BOSR34–38	—
CH271-171B20	InvHSA9	Chr9:27166326–27166532	Chr9:32479611–32479185	BOSR35	1Ov
CH271-202N11	InvHSA10	Chr10:51751886–51751461	Chr10:52229635–52229449	BOSR40	3Ov
CH271-185K6	InvHSA14	Chr14:30838138–30838392	Chr14:73124459–73124155	BOSR51–52	4Ov
CH271-133C19	InvHSA17	Chr17:26245998– 26246406	Chr17:27546961– 27546547	BOSR56	—
CH271-26L7	InvHSA17	Chr17:30504813–30504628	Chr17:45966506–45966963	BOSR57–58	3Ov
CH271-49C12	InvHSA17	Chr17:45884374–45884707	Chr17:55503126–55502460	BOSR58	—
CH271-219C17	InvHSA17	Chr17:20613964–20614099	Chr17:57510580–57511059	BOSR59	—
CH271-188I7	InvHSA19	Chr19:51714530–51714491	Chr19:5879587–5879508	BOSR62	—
CH271-30L2	InvHSA19	Chr19:5851377–5851846	Chr19:51500098–51500471	BOSR62	—
CH271-244C18	InvHSA6	Chr6:26666078–26866078	Chr6:58078211–58278211	BOSR20	—
CH271-286K22	InvHSA7	Chr7:75671223–75671763	Chr7:101829081–101830139	BOSR28–31	—
CH271-446I8	InvHSA7	Chr7:23083034–23082855	Chr7:67941088–67941258	BOSR27-cen	—
CH271-398E1	InvHSA17	Chr17:20753351–20754086	Chr17:69796739–69797427	—	6Ov; Ov CH271-262G5, 274L1

Additional gibbon clones spanning breakpoints were identified using the map of BOSRs obtained by array painting. Probes were designed inside the BOSRs and used to screen the gibbon genomic BAC library.
doi:10.1371/journal.pgen.0020223.t005

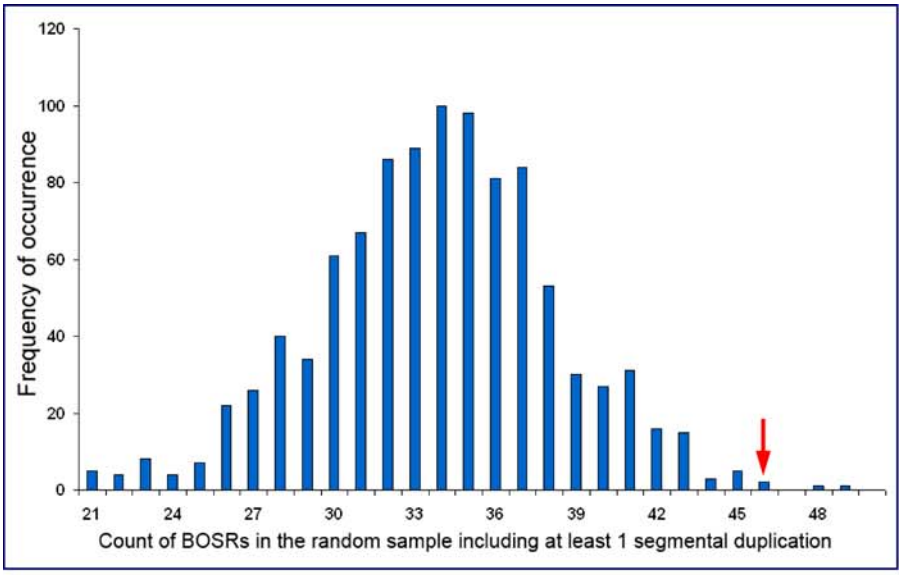
Frequency of occurrence
120
100
80
60
40
20
0
21
24
27
30
33
36
39
42
45
48
Count of BOSRs in the random sample including at least 1 segmental duplication

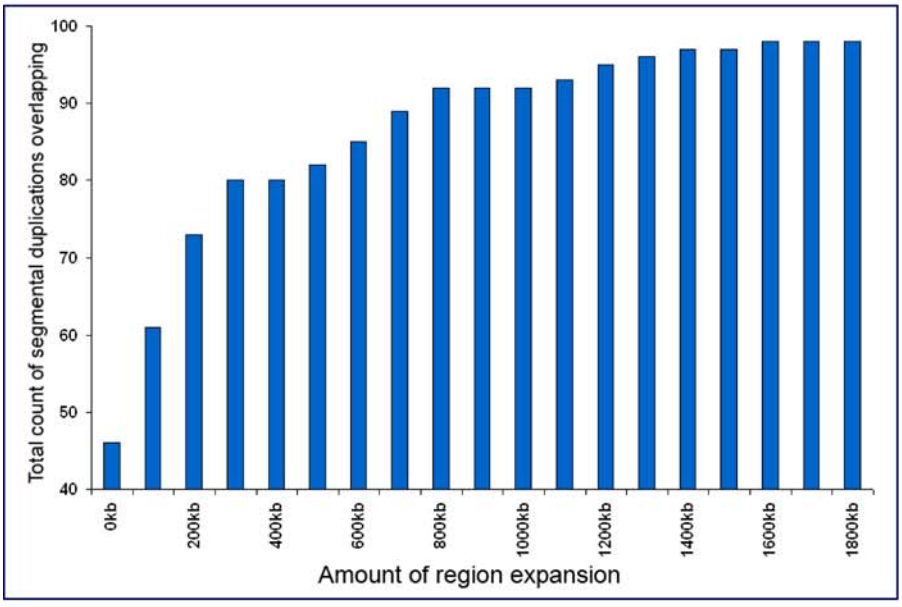
Total count of segmental duplications overlapping
100
90
80
70
60
50
40
0kb
200kb
400kb
600kb
800kb
1000kb
1200kb
1400kb
1600kb
1800kb
Amount of region expansion

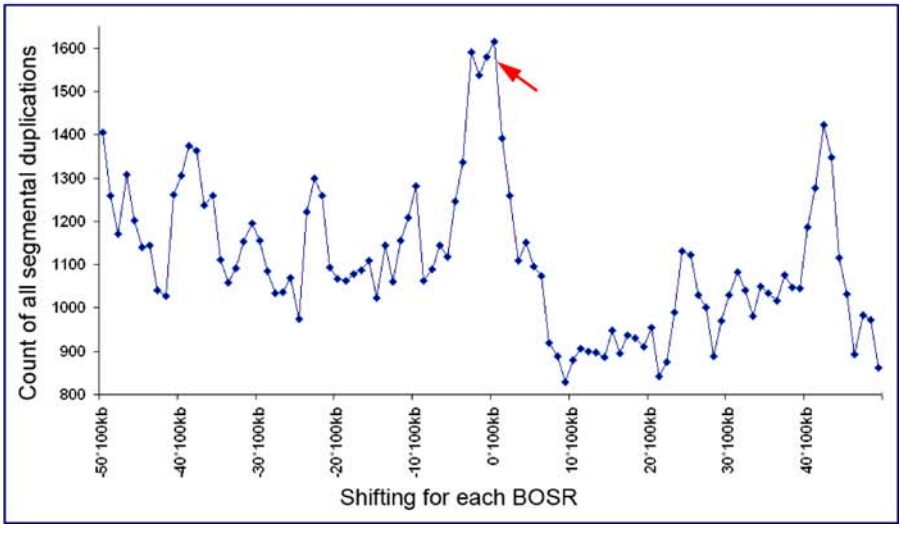
Count of all segmental duplications
1600
1500
1400
1300
1200
1100
1000
900
800
-50*100kb
-40*100kb
-30*100kb
-20*100kb
-10*100kb
0*100kb
10*100kb
20*100kb
30*100kb
40*100kb
Shifting for each BOSR

Figure 4. Association of the Breakpoint Regions with Segmental Duplication

(A) The figure shows the sampling distribution of the overlap between SDs and a random set of regions obtained by relocating our original sample 1,000 times in the corresponding chromosomes. The original sample fell more than three standard deviations away from the mean of the simulated distribution (red arrow).

(B) The regions from the original sample were expanded in 100 kb increments. The number of regions overlapping with SDs at each step is shown.

(C) We measured the amount of overlap (in base pairs) of our 100 regions, while shifting each of them up to 5 Mb left and right of their original positions in 100 kb increments. The strong correlation between the original position (red arrow) and SD content is shown.

doi:10.1371/journal.pgen.0020223.g004

centromere (Figure 5). Clones CH271-228C1 and CH271-86M19 span the reciprocal breakpoints of a translocation between human Chromosomes 7 and 20. In both clones, an (AT)n repeat separates the two homologous segments, preventing us from localizing the junction to the base-pair level. The (AT)n repeat in clone CH271-228C1 is 300 bp, and in CH271-86M19 it is 168 bp. A simple repeat classified as "AT rich" is also present in the corresponding position of human Chromosome 7. We confirmed the ancestral origin of this repeat by PCR amplifying and sequencing the orthologous region in gibbons belonging to three additional genera (*Hylobates agilis*, *Bunopithecus hoolock*, and *S. syndactylus*). We could therefore exclude the possibility that the repeat was a consequence of the rearrangement.

The presence of the AT-rich repeat in relation to these BOSRs may indicate a different breakpoint-inducing mechanism. Recently, Gotter and colleagues showed that the propensity to form secondary structures such as stem-loops can confer fragility to DNA [41]. Using the M-Fold sequence analysis package (http://bioweb.pasteur.fr/seqanal/interfaces/mfold-simple.html), we confirmed that the AT-rich repeats from the three clones give rise to long stem-loop structures (data not shown). At this point we do not have enough data to assume that this was the mechanism responsible for the translocation occurring during the evolution of the *Nomascus* genus. However, the cooccurrence of an evolutionary breakpoint and an AT-rich repeat region is intriguing.

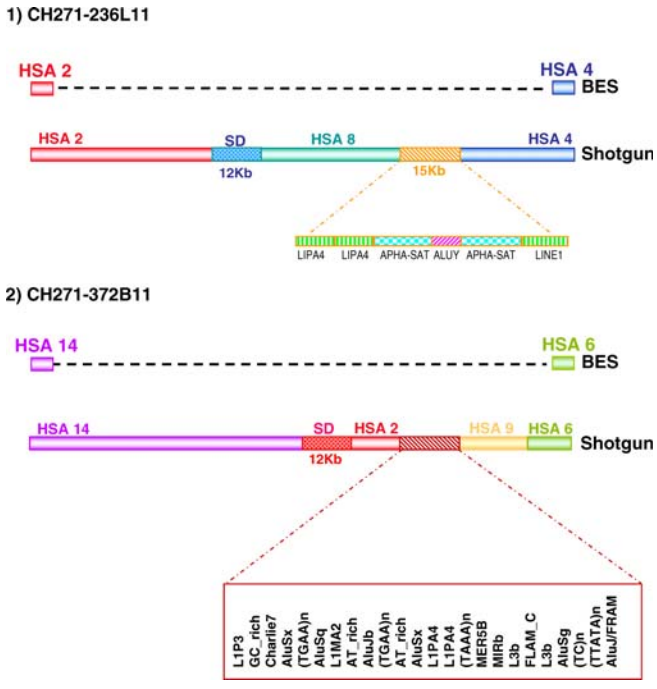

Figure 5. Analysis of Fully Sequenced Gibbon BAC Clones

Two sequenced gibbon clones spanning rearrangement breakpoints revealed the presence of additional segments of synteny not observed by other methods. In both cases, the first break of synteny was found to contain SDs and the second to contain interspersed repeats.

doi:10.1371/journal.pgen.0020223.g005

Conclusion

This study describes the mapping and validation of a large number of syntenic breakpoints between homologous chromosomes of human and NLE. All the translocation breakpoints previously identified by chromosome-painting studies were mapped to the human genome at a greatly increased resolution. About 20 additional rearrangements were discovered as a result of the higher sensitivity of our approaches. Overall, our research identified about 100 breakpoints occurring in the gibbon lineage. The study also yielded gibbon BACs containing breakpoint sites. In 11 sequenced gibbon BACs, we found elements near the breakpoints previously shown to play a key role in primate chromosome plasticity and evolution. Within the sequenced BACs three different patterns were evident. First, two BACs contained additional breakpoints that may have resulted from a complex, nonreciprocal translocation event or from subsequent chromosomal rearrangements. Recent high-resolution breakpoint analyses on human translocations thought to be balanced showed various "microtranslocations" [42]. Thus, translocations in human pathology and primate evolution may not always be simple breaks involving just two chromosomes but may be more complicated. Second, a correlation between SDs and evolutionary breakpoints in primates and other mammals has previously been suggested [11,13,16,43]. When all 100 gibbon-specific breakpoints were analyzed, a strong enrichment for SDs (in the human genome) was observed within 200 kb of the actual breakpoints (in the gibbon genome). Third, interspersed repeats have been linked to genomic instability in other studies, and several evolutionary breakpoints in primates are known to have occurred in repeat-rich areas [21,38,44,45]. Two of the sequenced BACs contained a breakpoint immediately adjacent to an AT-rich repeat with the potential to form stem-loop structures [41].

No generalized pattern unique to gibbon breakpoints is evident from the present molecular data. It remains to be determined if the greater number of chromosomal rearrangements in the small apes is due to an enhanced frequency of chromosomal breakages or an increased ability to rescue derivative chromosomes in comparison to other mammals, possibly due to mating behavior or inbreeding. We believe that these questions may be answered by examining additional aspects of small ape biology such as behavioral factors and population dynamics.

Materials and Methods

Array painting. BACs (32,855) spanning 95% of the human euchromatic genome were assembled and rearrayed into 384-well microtiter dishes [46,47]. DNA was purified, amplified using the DOP (degenerate oligonucleotide-primed) PCR method, and spotted on CMT-GAPS UltraGaps coated glass slides (Corning, www.corning.com). Gibbon chromosomes were sorted on a FACS Vantage flow

cytometry system (BD Biosciences, www.bdbiosciences.com) as described for previous experiments [31]. The NLE lymphoblast cell line used for chromosome sorting was the same as described by Müller et al. [31] and Schröck et al. [48]. Karyotype analysis revealed homozygosity for a known translocation polymorphism involving gibbon Chromosomes 1 and 22 (forms 1b and 22b). The only culture artifact observed was a trisomy for gibbon Chromosome 14. However, our karyotype analysis does not exclude the possibility that a small fraction of rearrangements observed by array painting were caused by cell-culture artifacts. DOP-amplified DNA [49] from flow-sorted chromosomes were subjected to a secondary DOP PCR and labeled with Cy3-dUTP (Amersham Biosciences, www5.amershambiosciences.com). Chromosomes X and Y were not included in this analysis because these are not involved in gibbon evolutionary translocations based on chromosome-painting studies. Anonymous human reference DNA was obtained from Children's Hospital Oakland Research Institute and amplified by DOP PCR. Labeling and hybridization were performed essentially as described by [50]. Hybridization images were generated by scanning the slides on a 4000B scanner (Axon Instruments, http://www.moleculardevices.com). The images were first processed using GenePix Pro 5.1 (Axon Instruments). The primary experimental data (GenePix Results files) were subjected to fully standardized data analysis (flagged spots removal, background subtraction, and loess normalization) by uploading them to the BioArray Software Environment microarray analysis software installation [51], which performs standard normalization. The final output was human chromosome specific plots of Log_2 ratio values versus chromosome location as well as a whole-genome view.

FISH. FISH was used as a validation method for BOSRs identified uniquely by array painting or for gibbon BACs spanning inversions. Metaphase preparations of NLE were obtained from the same cell line used for chromosome sorting and previously described by Müller et al. [31] and Schröck et al. [48]. The cell lines used for metaphase preparations of HLA and *S. syndactylus* were the ones described by Jauch et al. [25] and Koehler et al. [26], respectively. *Homo sapiens* (HSA) metaphase preparations were prepared from peripheral blood culture.

BAC DNA extraction was performed as reported by Ventura et al. [25]. FISH experiments were performed essentially as described by Lichter et al. [52]. BACs were labeled either with biotin-dUTP or digoxigenin-dUTP by standard nick-translation assay. Fluorescent signals were obtained using avidin-FITC (Vector Laboratories, www.vectorlabs.com) and anti-digoxigenin-rhodamine antibodies (Roche, http://www.roche-diagnostics.com). When confirming translocation breakpoints on gibbon chromosomes, BACs were hybridized together with chromosome-specific painting probes obtained from sorting lymphoblastoid and somatic hybrid cell line chromosomes followed by DOP PCR [52]. Digital images were obtained using a Zeiss Axioskop (Carl Zeiss Inc., www.zeiss.com) microscope equipped with a CCD-1300DS (VDS Vosskuehler GmbH, www.vdsvossk.de) or a SenSys (Photometrics, www.photomet.com) cooled CCD camera. Pseudocoloring and merging of images was performed using SmartCapture (Digital Scientific, www.digitalscientific.co.uk) or Adobe Photoshop software (Adobe Systems Inc, www.adobe.com).

Library screenings. To identify BACs spanning putative breakpoint regions, overgo probes of 40 bp [53] were designed from end sequences of selected gibbon BAC clones. To search for reciprocal breakpoints, the overgo probes were designed from the human sequence at 170 kb from the BES location. All the probes were pooled together and hybridized to high-density filters of the CHORI-271 library following procedures already described [54]. Subsequently, the positive clones obtained from this first screening were rearrayed on small filters. Each small filter was used for hybridization with individual probes.

The images were analyzed with the software ArrayVision Ver6.0 (Imaging Research Inc., www.imagingresearch.com).

Supporting Information

Figure S1. Identification of BOSRs between Human and Gibbon Chromosomes by Array Painting

The results of array painting experiments done with different pools were combined for each human chromosome. After applying the difference method for noise reduction (see text) we identified all 64 BOSRs at a resolution of 300 kb (average) with the employment of a limited number of experiments. The figure shows the results obtained for all human chromosomes.

Found at doi:10.1371/journal.pgen.0020223.sg001 (240 MB PPT).

Figure S2. Translocations Viewer

This tool was developed in order to easily localize gibbon clones spanning a translocation or inversion breakpoint in human. Figure S2A corresponds to a full genome view and Figure S2B corresponds to Chromosome 16. Gibbon clones are represented by the blue arrows, taking into account the orientation of each BES. On the bottom of the window is a density plot of human SDs.

Found at doi:10.1371/journal.pgen.0020223.sg002 (493 KB PPT).

Figure S3. Interphase FISH Experiments to Show Duplications in Gibbon

A sample of gibbon BAC clones overlapping human SDs was hybridized on NLE nuclei. The presence of duplications was revealed by the presence of either multiple signals or a single but broadened signal. The figure shows the results obtained with four clones also tested on HLA and *S. syndactylus*.

Found at doi:10.1371/journal.pgen.0020223.sg003 (122 KB JPG).

Protocol S1.

Found at doi:10.1371/journal.pgen.0020223.sd001 (41 KB DOC).

Table S1. Composition of Gibbon Sorted Chromosome Pools for Array-Painting Experiments

The gibbon chromosomes were divided into four pools in order to minimize the number of array-painting experiments. A smart-pooling strategy was used, taking advantage of the data available in the literature. Through this approach the repetition of one human chromosome in the same pool was avoided. Additionally, three gibbon chromosomes were hybridized in individual experiments.

Found at doi:10.1371/journal.pgen.0020223.st001 (45 KB DOC).

Table S2. Comparative Mapping of Gibbon Clones Spanning Breakpoints on Rhesus Macaque and Chimpanzee Genome Assemblies

The table reports the outcome of the mapping of gibbon clones spanning BOSRs on the latest genome assembly of Rhesus macaque (reMach2) and chimpanzee (panTro1). Depending on the result, clones were classified into three evolutionary groups: 1) gibbon specific, 2) great ape specific, and 3) human specific.
Mapping results not consistent with human are in italics.

Found at doi:10.1371/journal.pgen.0020223.st002 (134 KB DOC).

Accession numbers

The National Center for Biotechnology Information (NCBI) Entrez Gene (http://www.ncbi.nlm.nih.gov/entrez/query.fcgi?db=gene) accession numbers for the genes discussed in this paper are *CASP1* (NM__033294), *CASP4* (837), *CASP5* (838), *GH2* (2689), *KRTAP5–10* (387273), *KRTAP5–11* (440051), *KRTAP5–7* (440050), *KRTAP5–8* (57830), *KRTAP5–9* (3846), *MRC1* (4360), *OR11L1* (391189),*OR13G1* (441933), *OR1C1* (26188), *OR2G2* (81470), *OR2G3* (81469), *OR5AT1* (284532), and *OR6F1* (343169).

Acknowledgments

We are extremely grateful to Dr. Ulli Weier and his group at Lawrence Berkeley National Laboratory for making their facilities available to us. We are also thankful to Dr. Yuko Yoshinaga for help in managing communications with the sequencing agency for the gibbon BAC end sequencing. We finally thank BACPAC Resources for their help with the production of the rearrayed filters employed in the secondary screenings.

Author contributions. LC and PJdJ conceived and designed the experiments. LC, AK, and JW performed the experiments. GMV, CS, RAH, and AM analyzed the data. BFHtH, BZ, KO, AM, JW, JR, and SH contributed reagents/materials/analysis tools. LC, GMV, and PJdJ wrote the paper.

Funding. Construction and characterization of CHORI-271 gibbon BAC library was supported by a National Institutes of Health grant (HG02523–02) to PJdJ.

Competing interests. The authors have declared that no competing interests exist.

References

1. Wienberg J (2004) The evolution of eutherian chromosomes. Curr Opin Genet Dev 14: 657–666.
2. Gregory SG, Sekhon M, Schein J, Zhao S, Osoegawa K, et al. (2002) A physical map of the mouse genome. Nature 418: 743–750.
3. Nadeau JH, Taylor BA (1984) Lengths of chromosomal segments conserved since divergence of man and mouse. Proc Natl Acad Sci U S A 81: 814–818.
4. Lindblad-Toh K, Wade CM, Mikkelsen TS, Karlsson EK, Jaffe DB, et al. (2005) Genome sequence, comparative analysis and haplotype structure of the domestic dog. Nature 438: 803–819.
5. Zhao S, Shetty J, Hou L, Delcher A, Zhu B, et al. (2004) Human, mouse, and rat genome large-scale rearrangements: stability versus speciation. Genome Res 14: 1851–1860.
6. Dutrillaux B, Rethore MO, Aurias A, Goustard M (1975) [Karyotype analysis of 2 species of *gibbons (Hylobates lar and H. concolor)* with different banding species]. Cytogenet Cell Genet 15: 81–91.
7. Koehler U, Bigoni F, Wienberg J, Stanyon R (1995) Genomic reorganization in the concolor gibbon *(Hylobates concolor)* revealed by chromosome painting. Genomics 30: 287–292.
8. Mrasek K, Heller A, Rubtsov N, Trifonov V, Starke H, et al. (2003) Detailed *Hylobates lar* karyotype defined by 25-color FISH and multicolor banding. Int J Mol Med 12: 139–146.
9. Armengol L, Pujana MA, Cheung J, Scherer SW, Estivill X (2003) Enrichment of segmental duplications in regions of breaks of synteny between the human and mouse genomes suggest their involvement in evolutionary rearrangements. Hum Mol Genet 12: 2201–2208.
10. Ventura M, Mudge JM, Palumbo V, Burn S, Blennow E, et al. (2003) Neocentromeres in 15q24–26 map to duplicons which flanked an ancestral centromere in 15q25. Genome Res 13: 2059–2068.
11. Bailey JA, Baertsch R, Kent WJ, Haussler D, Eichler EE (2004) Hotspots of mammalian chromosomal evolution. Genome Biol 5: R23.
12. Newman TL, Tuzun E, Morrison VA, Hayden KE, Ventura M, et al. (2005) A genome-wide survey of structural variation between human and chimpanzee. Genome Res 15: 1344–1356.
13. Murphy WJ, Larkin DM, Everts-van der Wind A, Bourque G, Tesler G, et al. (2005) Dynamics of mammalian chromosome evolution inferred from multispecies comparative maps. Science 309: 613–617.
14. Goidts V, Szamalek JM, Hameister H, Kehrer-Sawatzki H (2004) Segmental duplication associated with the human-specific inversion of chromosome 18: A further example of the impact of segmental duplications on karyotype and genome evolution in primates. Hum Genet 115: 116–122.
15. Stankiewicz P, Park SS, Inoue K, Lupski JR (2001) The evolutionary chromosome translocation 4;19 in *Gorilla goril*la is associated with microduplication of the chromosome fragment syntenic to sequences surrounding the human proximal CMT1A-REP. Genome Res 11: 1205–1210.
16. Locke DP, Archidiacono N, Misceo D, Cardone MF, Deschamps S, et al. (2003) Refinement of a chimpanzee pericentric inversion breakpoint to a segmental duplication cluster. Genome Biol 4: R50.
17. Eder V, Ventura M, Ianigro M, Teti M, Rocchi M, et al. (2003) Chromosome 6 phylogeny in primates and centromere repositioning. Mol Biol Evol 20: 1506–1512.
18. Casals F, Caceres M, Ruiz A (2003) The foldback-like transposon Galileo is involved in the generation of two different natural chromosomal inversions of *Drosophila buzzatii*. Mol Biol Evol 20: 674–685.
19. Lim JK, Simmons MJ (1994) Gross chromosome rearrangements mediated by transposable elements in *Drosophila melanogaster*. Bioessays 16: 269–275.
20. Lee JW, Kim HS (2006) Endogenous retrovirus HERV-I LTR family in primates: Sequences, phylogeny, and evolution. Arch Virol 151: 1651–1658.
21. Kehrer-Sawatzki H, Schreiner B, Tanzer S, Platzer M, Müller S, et al. (2002) Molecular characterization of the pericentric inversion that causes differences between chimpanzee chromosome 19 and human chromosome 17. Am J Hum Genet 71: 375–388.
22. Van Tuinen P, Ledbetter DH (1983) Cytogenetic comparison and phylogeny of three species of Hylobatidae. Am J Phys Anthropol 61: 453–466.
23. Stanyon R, Sineo L, Chiarelli B, Camperio-Ciani A, Mootnick AR, et al. (1987) Banded karyotypes of the 44-chromosomes gibbons. Folia Primatol 48: 56–64.
24. Prouty LA, Buchanan PD, Pollitzer WS, Mootnick AR (1983) A presumptive new hylobatid subgenus with 38 chromosomes. Cytogenet Cell Genet 35: 141–142.
25. Jauch A, Wienberg J, Stanyon R, Arnold N, Tofanelli S, et al. (1992) Reconstruction of genomic rearrangements in great apes and gibbons by chromosome painting. Proc Natl Acad Sci U S A 89: 8611–8615.
26. Koehler U, Arnold N, Wienberg J, Tofanelli S, Stanyon R (1995) Genomic reorganization and disrupted chromosomal synteny in the siamang (*Hylobates syndactylus*) revealed by fluorescence in situ hybridization. Am J Phys Anthropol 97: 37–47.
27. Yu D, Yang F, Liu R (1997) [A comparative chromosome map between human and Hylobates hoolock built by chromosome painting]. Yi Chuan Xue Bao 24: 417–423.
28. Nie W, Rens W, Wang J, Yang F (2001) Conserved chromosome segments in *Hylobates hoolock* revealed by human and *H. leucogenys* paint probes. Cytogenet Cell Genet 92: 248–253.
29. Müller S, Hollatz M, Wienberg J (2003) Chromosomal phylogeny and evolution of gibbons (Hylobatidae). Hum Genet 113: 493–501.
30. Arnold N, Stanyon R, Jauch A, O'Brien P, Wienberg J (1996) Identification of complex chromosome rearrangements in the gibbon by fluorescent in situ hybridization (FISH) of a human chromosome 2q specific microlibrary, yeast artificial chromosomes, and reciprocal chromosome painting. Cytogenet Cell Genet 74: 80–85.
31. Müller S, O'Brien PC, Ferguson-Smith MA, Wienberg J (1998) Cross-species colour segmenting: A novel tool in human karyotype analysis. Cytometry 33: 445–452.
32. Gribble SM, Fiegler H, Burford DC, Prigmore E, Yang F, et al. (2004) Applications of combined DNA microarray and chromosome sorting technologies. Chromosome Res 12: 35–43.
33. Volik S, Zhao S, Chin K, Brebner JH, Herndon DR, et al. (2003) End-sequence profiling: Sequence-based analysis of aberrant genomes. Proc Natl Acad Sci U S A 100: 7696–7701.
34. Kent WJ (2002) BLAT—the BLAST-like alignment tool. Genome Res 12: 656–664.
35. Yue Y, Grossmann B, Ferguson-Smith M, Yang F, Haaf T (2005) Comparative cytogenetics of human chromosome 3q21.3 reveals a hot spot for ectopic recombination in hominoid evolution. Genomics 85: 36–47.
36. Müller S, Finelli P, Neusser M, Wienberg J (2004) The evolutionary history of human chromosome 7. Genomics 84: 458–467.
37. Bailey JA, Gu Z, Clark RA, Reinert K, Samonte RV, et al. (2002) Recent segmental duplications in the human genome. Science 297: 1003–1007.
38. Kehrer-Sawatzki H, Sandig CA, Goidts V, Hameister H (2005) Breakpoint analysis of the pericentric inversion between chimpanzee chromosome 10 and the homologous chromosome 12 in humans. Cytogenet Genome Res 108: 91–97.
39. Bailey JA, Yavor AM, Massa HF, Trask BJ, Eichler EE (2001) Segmental duplications: Organization and impact within the current human genome project assembly. Genome Res 11: 1005–1017.
40. Ye C, Li Y, Shi P, Zhang YP (2005) Molecular evolution of growth hormone gene family in old world monkeys and hominoids. Gene 350: 183–192.
41. Gotter AL, Shaikh TH, Budarf ML, Rhodes CH, Emanuel BS (2004) A palindrome-mediated mechanism distinguishes translocations involving LCR-B of chromosome 22q11.2. Hum Mol Genet 13: 103–115.
42. Fauth C, Gribble SM, Porter KM, Codina-Pascual M, Ng BL, et al. (2006) Micro-array analyses decipher exceptional complex familial chromosomal rearrangement. Hum Genet 119: 145–153.
43. Kurahashi H, Inagaki H, Ohye T, Kogo H, Kato T, et al. (2006) Chromosomal translocations mediated by palindromic DNA. Cell Cycle 5: 1297–1303.
44. Coghlan A, Eichler EE, Oliver SG, Paterson AH, Stein L (2005) Chromosome evolution in eukaryotes: A multi-kingdom perspective. Trends Genet 21: 673–682.
45. Goidts V, Szamalek JM, Jong PJd, Cooper DN, Chuzhanova N, et al. (2005) Independent intra-chromosomal recombination events underlie the pericentric inversions of chimpanzee and gorilla chromosomes homologous to human chromosome 16. Genome Res 15: 1232–1242.
46. Ishkanian AS, Malloff CA, Watson SK, DeLeeuw RJ, Chi B, et al. (2004) A tiling resolution DNA microarray with complete coverage of the human genome. Nat Genet 36: 299–303.
47. Krzywinski M, Bosdet I, Smailus D, Chiu R, Mathewson C, et al. (2004) A set of BAC clones spanning the human genome. Nucleic Acids Res 32: 3651–3660.
48. Schröck E, du Manoir S, Veldman T, Schoell B, Wienberg J, et al. (1996) Multicolor spectral karyotyping of human chromosomes. Science 273: 494–497.
49. Telenius H, Carter NP, Bebb CE, Nordenskjold M, Ponder BA, et al. (1992) Degenerate oligonucleotide-primed PCR: General amplification of target DNA by a single degenerate primer. Genomics 13: 718–725.
50. Veltman JA, Schoenmakers EF, Eussen BH, Janssen I, Merkx G, et al. (2002) High-throughput analysis of subtelomeric chromosome rearrangements by use of array-based comparative genomic hybridization. Am J Hum Genet 70: 1269–1276.
51. Saal LH, Troein C, Vallon-Christersson J, Gruvberger S, Borg A, et al. (2002) BioArray Software Environment (BASE): A platform for comprehensive management and analysis of microarray data. Genome Biol 3: SOFTWARE0003.
52. Lichter P, Ledbetter SA, Ledbetter DH, Ward DC (1990) Fluorescence in situ hybridization with Alu and L1 polymerase chain reaction probes for rapid characterization of human chromosomes in hybrid cell lines. Proc Natl Acad Sci U S A 87: 6634–6638.
53. McPherson JD, Marra M, Hillier L, Waterston RH, Chinwalla A, et al. (2001) A physical map of the human genome. Nature 409: 934–941.
54. Osoegawa K, Tateno M, Woon PY, Frengen E, Mammoser AG, et al. (2000) Bacterial artificial chromosome libraries for mouse sequencing and functional analysis. Genome Res 10: 116–128.